An Upwind-Euler scheme for an ODE-PDE model of supply chains

Alfredo Cutolo [(1)], Benedetto Piccoli [(2)], Luigi Rarità [(1)]
[(1)]Department of Information Engineering and Applied Mathematics,
University of Salerno, Fisciano (SA), Italy
[(2)]Istituto per le Applicazioni del Calcolo "Mauro Picone",
Consiglio Nazionale delle Ricerche, Roma, Italy

August 30, 2010

Abstract

Numerical techniques for the simulation of an ODE-PDE model for supply chains are presented. First we describe a scheme, based on Upwind and explicit Euler methods, provide corrections to maintain positivity of solutions, prove convergence and provide convergence rate. The latter is achieved via comparison with Wave Front Tracking solutions and the use of generalized tangent vectors. Different choice of time and space meshes give similar results, both for CPU times and numerical errors. Fast algorithms, based on an accurate choice of time and space meshes and data structures, are then proposed, achieving high computational gains.

1 Introduction

In last years, scientific communities showed a great interest in modelling dynamics of industrial productions, managed by supply chains. This study is fundamental in order to reduce some unwished phenomena (bottlenecks, dead times, and so on).

Several mathematical approaches have been proposed. For example, some models are discrete and based on considerations of individual parts (for a review, see [10]). Other models are continuous ([1, 2, 3, 24]), and some based on partial differential equations. The first paper in this last direction was [1], where the authors, via a limit procedure on the number of parts and suppliers, have obtained a conservation law formulation. The flux involves parts density and the maximal productive capacity. The main problem is that solutions for discontinuous productive capacity functions may exhibit delta waves. For this reason, alternative models were proposed. For instance, a mixed continuum-discrete model is given in [11]: The supply chain is described by continuous arcs and discrete nodes. Also extensions on networks have been made ([12, 13, 14]).

In this paper, we focus the attention on the continuous model for supply chains and networks proposed by Göttlich, Herty and Klar in [17]. Our main aim is to analyze the convergence of the Upwind-Euler scheme and improve its performance by accurate choice of discretization parameters. Examples of schemes for conservation laws on networks can

be found in [6, 17, 20]. The necessity of having fast numerics is justified by optimization problems which arise naturally in applications, see [18, 22].
The model of [17] is obtained considering suppliers on which the processing rate is constant (thus avoiding the problem of delta waves) and having queues in front of each supplier. The evolution of the queue buffer occupancy is given by the difference of fluxes from the preceding and following suppliers. The outcome is a coupled ODE-PDE model.
Two numerical schemes must be considered: One for the ODE and one for the PDE. We choose the Upwind method for parts densities, described by conservation laws (PDEs), and the explicit Euler scheme for queue evolutions, modelled by ODEs. For details, see also [16] and [23].

Notice that the ODE-PDE model guarantees positivity of queue buffer occupancies (and densities), while this is not granted for the Upwind-Euler scheme. Thus first we consider fluxes corrections to avoid this drawback.
The choice of time and space meshes can be uniform over suppliers only in case of rational ratios among lengths. Thus we consider different discretizations of the Upwind-Euler to deal with the general case and also to reduce computational complexity.
Convergence of the scheme is proved using a comparison with Wave Front Tracking approximate solutions. More precisely, we consider nesting grids in which meshes are divided by two in successive approximations. Then generalized tangent vectors, as in [21], are defined and the evolution of their norms permits to bound L^1 distances of solutions. Finally, a linear convergence rate is achieved in terms of the space (or time) mesh. A similar technique was used in [8] to prove convergence for an ODE-PDE (not completely coupled) model to track the trajectory of a car on a road network.

From several simulations of supply chains, it is evident that heavy numerical errors occur if corrections for negative queues are not adopted. Moreover, different time-space discretizations for the Upwind-Euler method perform similarly, both in terms of CPU times and numerical errors.
Focusing on the last point, computational gains are obtained by the use of logic pointers to update the computed density values. This allows a strong reduction of computational complexity as shown by simulation of relatively large supply chains (10 and 100 arcs), for which CPU times reduce of up to 90%.

The outline of the paper is the following. In Section 2, we present the ODE-PDE model. Then Section 3 describes the Upwind-Euler scheme, while its convergence is proven in Section 4, shifting to the Appendix the description of generalized tangent vectors. Section 5 reports tests showing the importance of positivity of solutions. Reduction of computational complexity is addressed in Section 6 and the relative numerical tests are described in Section 7.

2 A model for supply chains

In this section, we present an ODE-PDE model for supply chains first proposed in [17], and based on the work [1]. Beside the conservation laws formulation proposed in [1], such model includes time - dependent queues describing the transition of parts among suppliers.

A supply chain is a directed graph consisting of arcs $\mathcal{J} = \{1, ..., N\}$ and vertices

$\mathcal{V} = \{1, ..., N-1\}$. Each arc $j \in \mathcal{J}$, parameterized by an interval $[a_j, b_j]$, models a supplier. Each vertex is connected to one incoming arc and one outgoing arc and we assume that arcs are consecutively labelled, i.e. arc j is connected to arc $j+1$ and $b_j = a_{j+1}$ (see Figure 1). For the first and the last arc, we either set $a_1 = -\infty$ and $b_N = +\infty$, respectively, or provide boundary data for the inflow and outflow.

Each supplier j has a queue in front of itself, i.e. at $x = a_j$, and is characterized by a

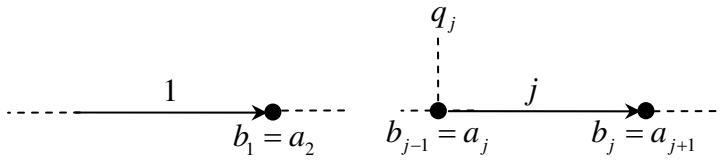

Figure 1: an example of supply chain.

maximum processing capacity $\mu_j > 0$, length $L_j > 0$ and a processing time $T_j > 0$. The rate L_j/T_j represents the processing velocity. Indicating by $\rho_j(t,x)$ the density of parts in the supplier j at point x and time t, the evolution of parts is described by a conservation law:

$$\partial_t \rho_j(t,x) + \partial_x f_j(\rho_j(t,x)) = 0, \quad \forall\, x \in [a_j, b_j], \quad t > 0, \tag{1}$$

where the flux function $f_j(\rho_j(t,x))$ is given by:

$$f_j : [0, +\infty[\to [0, \mu_j], \quad f_j(\rho_j(t,x)) = \min\left\{\mu_j, \frac{L_j}{T_j}\rho_j(t,x)\right\}.$$

The interpretation of equation (1) is the following: Parts are processed with velocity L_j/T_j but with a maximal flux μ_j.

Each queue buffer occupancy is a time dependent function $t \to q_j(t)$. If the capacity of the supplier $j-1$ and the demand of the supplier j are not equal, the queue increases or decreases its buffer. More precisely, we have:

$$\frac{d}{dt}q_j(t) = f_{j-1}(\rho_{j-1}(b_{j-1}, t)) - f_j(\rho_j(a_j, t)), \quad j = 2, ..., N, \tag{2}$$

$$q_j(0) = q_{j,0} \geq 0,$$

where $f_{j-1}(\rho_{j-1}(b_{j-1}, t))$ is defined by the evolution on supplier $j-1$, while the flux on the outgoing arc j is defined as

$$f_j(\rho_j(a_j, t)) = \begin{cases} \min\{f_{j-1}(\rho_{j-1}(b_{j-1}, t)), \mu_j\}, & q_j(t) = 0, \\ \mu_j, & q_j(t) > 0. \end{cases} \tag{3}$$

Notice that the flux $f_j(\rho_j(a_j, t))$ depends on the capacity of the queue: If the queue buffer is empty, the inflow to supplier j is equal to the outflow from supplier $j-1$, otherwise the inflow is maximal. In other words, when there are parts in the queue the processing

occurs at the maximal possible rate, namely μ_j, so to empty the queue as fast as possible. Finally, the complete system of equations is:

$$\partial_t \rho_j(t,x) + \partial_x \min\left\{\mu_j, \frac{L_j}{T_j}\rho_j(t,x)\right\} = 0, \ \forall\ x \in [a_j, b_j], \quad t > 0, \quad j \in \mathcal{J}, \tag{4}$$

$$\rho_j(0,x) = \rho_{j,0}(x) \geq 0, \quad \forall\ x \in [a_j, b_j], \tag{5}$$

$$\frac{d}{dt} q_j(t) = f_{j-1}\left(\rho_{j-1}(b_{j-1}, t)\right) - f_j\left(\rho_j(a_j, t)\right), \ j = 2, ..., N, \tag{6}$$

$$q_j(0) = q_{j,0} \geq 0, \tag{7}$$

$$f_j\left(\rho_j(a_j,t)\right) = \begin{cases} \min\{f_{j-1}\left(\rho_{j-1}(b_{j-1},t)\right), \mu_j\}, & q_j(t) = 0, \\ \mu_j, & q_j(t) > 0. \end{cases} \tag{8}$$

Lemma 1 *Consider a supply chain evolution $\rho_j(t,x)$, $q_j(t)$, i.e. a solution to (4)-(8). Then for every $j \in \mathcal{J}$, $t \geq 0$ and x, it holds $\rho_j(t,x) \geq 0$, $q_j(t) \geq 0$.*

Proof. Since the inflows (8) are positive and the fluxes f_j vanish at 0, the density parts ρ_j are always positive by comparison principle of conservation laws. Moreover (6) and (8) guarantee that the derivative of queue buffer occupancy is always positive when the queue is empty, thus the conclusion follows. ■

2.1 Supply networks.

The ODE-PDE model (4)-(8) can be extended to the case of networks, see [18]. The main idea is to introduce traffic distribution coefficients at nodes, which describe how the outgoing flux from a given node distribute over suppliers which are downstream.

More precisely, a network is a directed graph formed by a set of arcs $\mathcal{J}$ and a set of vertices $\mathcal{V}$. Each arc $j \in \mathcal{J}$, parameterized by an interval $[a_j, b_j]$, models a supplier (possibly having infinite endpoints) and there is a queue in front of it if $a_j > -\infty$. Each vertex v is connected to some incoming arcs and some outgoing arcs. On the other side each arc is outgoing for at most one vertex and is incoming for at most one vertex. More precisely j is outgoing for some vertex if $a_j > -\infty$ and is incoming for some vertex if $b_j < +\infty$. We indicate by $Inc(v) \subset J$ the set of incoming arcs into v and by $Out(v) \subset J$ the set of outgoing arcs from v. For each v there exist distributions coefficients $(a_{v,j})_{j \in Out(v)}$ such that $a_{v,j} \in]0,1[$ and $\sum_{j \in Out(v)} a_{j,v} = 1$. The coefficient $a_{v,j}$ represents the percentage of flux outgoing from v which is directed to the supplier j.

The model (4)-(8) can be modified as follows to deal with networks. Notice that (4), (5) and (7) have the same expression. Now fix a supplier j, with $a_j > -\infty$, and let v be the vertex such that $j \in Out(v)$. Equation (6) is replaced by:

$$\frac{d}{dt} q_j(t) = a_{v,j} f_v(t) - f_j\left(\rho_j(a_j,t)\right) \tag{9}$$

where

$$f_v(t) = \sum_{k \in Inc(v)} f_k\left(\rho_k(b_k,t)\right) \tag{10}$$

and (8) is replaced by:

$$f_j\left(\rho_j\left(a_j,t\right)\right)=\begin{cases}\min\{a_{v,j}f_v(t),\mu_j\}, & q_j\left(t\right)=0,\\ \mu_j, & q_j\left(t\right)>0.\end{cases} \tag{11}$$

Also in this case we have positivity of solutions, more precisely:

Lemma 2 *Consider a supply network evolution $\rho_j(t,x)$, $q_j(t)$, i.e. a solution to (4), (5), (7), (9), (10), (11). Then for every $j\in\mathcal{J}$, $t\geq 0$ and x, it holds $\rho_j(t,x)\geq 0$, $q_j(t)\geq 0$.*

Proof. Since $a_{j,v}>0$, the inflows (11) are positive and, as before, the fluxes f_j vanish at 0, thus the density parts ρ_j are always positive by comparison principle of conservation laws. Equations (9), (10) and (11) ensure that the derivative of queue buffer occupancy is always positive when the queue is empty, thus the conclusion follows. ■

3 The Upwind-Euler scheme

In this Section we introduce the Upwind-Euler method with various possible discretizations. For simplicity we focus on supply chains, being the case of networks entirely similar.

Numerical results for parts dynamics on a supply chain are obtained finding, for each arc j, suitable approximation for the density $\rho_j\left(t,x\right)$, and the queue buffer occupancy $q_j\left(t\right)$. In particular, we need a PDE numerical method and an ODE one: We choose the Upwind scheme for the PDE and the explicit Euler scheme for the ODE.
For each arc $j\in\mathcal{J}$, define a numerical grid in $[0,L_j]\times[0,T]$ using the following notations:

- $\Delta x_j=\frac{L_j}{N_j}$ is the space grid mesh, where N_j is the number of segments into which we divide the j-th supplier;
- $\Delta t_j=\frac{T}{\eta_j}$ is the time grid mesh, where η_j denotes the number of segments into which $[0,T]$ is divided;
- $\left(x_i,t^n\right)_j=\left(i\Delta x_j,\ n\Delta t_j\right)$, $i=0,...,N_j$, $n=0,...,\eta_j$ are the grid points;
- ${}^j\rho_i^n$ is the value taken by the approximated density at the point $\left(x_i,t^n\right)_j$;
- q_j^n is the value taken by the approximate queue buffer occupancy at time t^n.

The Upwind method reads:

$${}^j\rho_i^{n+1}={}^j\rho_i^n-\frac{\Delta t}{\Delta x}\frac{L_j}{T_j}\left({}^j\rho_i^n-{}^j\rho_{i-1}^n\right),\ j\in\mathcal{J},\ i=0,...,N_j,n=0,...,\eta_j, \tag{12}$$

with CFL condition given by

$$\Delta t\leq\frac{\Delta x}{\max_j\frac{L_j}{T_j}}, \tag{13}$$

while the explicit Euler method is given by:

$$q_j^{n+1}=q_j^n+\Delta t\left(f_{j-1,out}^n-f_{j,inc}^n\right),\ j\in\mathcal{J}\backslash\{1\},\ n=0,...,\eta_j, \tag{14}$$

where

$$f^n_{j-1,out} = f_{j-1}(^{j-1}\rho^n_{N_{j-1}}),$$

$$f^n_{j,inc} = \begin{cases} \min\left\{ f_{j-1}(^{j-1}\rho^n_{N_{j-1}}), \mu_j \right\}, & q^n_j(t) = 0, \\ \mu_j, & q^n_j(t) > 0. \end{cases} \tag{15}$$

Boundary data are treated using ghost cells and the expression of inflows given by (15).

Assuming that the numbers L_j have rational ratios, it is possible to choose a space grid mesh Δx and a common time grid mesh Δt. We will discuss below the general case.

3.1 Correction of numerical fluxes in case of negative queues

The ODE numerical scheme does not necessarily maintain the positivity properties of the true solutions given by Lemma 1. We thus modify the Euler scheme so as to accomplish positivity of queue buffer occupancies.

Consider a supplier j and a time interval $\left[t^n, t^{n+1}\right[$ so that $q^{n+1}_j < 0 < q^n_j$. Then we define $q_j(t)$ for every time t by linear interpolation, see Figure 2, namely

$$q_j(t) = \frac{q^{n+1}_j - q^n_j}{\Delta t} t + \frac{q^n_j t^{n+1} - q^{n+1}_j t^n}{\Delta t}, \quad t \in \left[t^n, t^{n+1}\right[. \tag{16}$$

Then $q(\cdot)$ vanishes at some time $\bar{t} > t^n$, which is computed by (16):

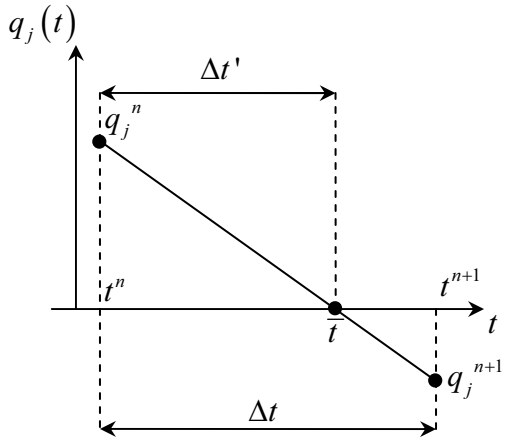

Figure 2: Negative queue buffer occupancy at t^{n+1}.

$$\bar{t} = t^n + \Delta t', \quad \Delta t' = \frac{q^n_j}{q^n_j - q^{n+1}_j} \Delta t = \frac{q^n_j}{\mu_j - f^n_{j-1,out}}. \tag{17}$$

Correcting to zero $q_j(t)$, $t \in \left[\bar{t}, t^{n+1}\right]$, the following numerical correction for the entering flux $f^n_{j,inc}$ is needed:

$$f^n_{j,inc} = \frac{1}{\Delta t}\left[\Delta t' \mu_j + \left(\Delta t - \Delta t'\right) f^n_{j-1,out}\right]. \tag{18}$$

The correction (18) on the boundary incoming data for the supplier j influences the approximation of $\rho_j(x,t)$, with consequent effects on the dynamics for following suppliers and queues.
We have the following (cfr. Lemma 1):

Lemma 3 *Consider a numerical solution ${}^j\rho_i^n$, q_j^n, defined using the flux correction (18), such that ${}^j\rho_i^0 \geq 0$ and $q_j^0 \geq$ for all $j \in \mathcal{J}$, $i = 1, \ldots, N_j$. Then ${}^j\rho_i^n \geq 0$, $q_j^n \geq 0$, for all $n \geq 0$, $j \in \mathcal{J}$, $i = 1, \ldots, N_j$.*

Proof. By formulas (12), (13) and (15), since ${}^j\rho_i^0 \geq 0$, for all $j \in \mathcal{J}$, $i = 1, \ldots, N_j$, we clearly have that ${}^j\rho_i^n \geq 0$, $q_j^n \geq 0$, for all $n \geq 0$, $j \in \mathcal{J}$, $i = 1, \ldots, N_j$.
Now if (14) gives rise to a negative value for some $j \in \mathcal{J}$ and $n \geq 1$, then using the flux correction (18), we can write:

$$q^{n+1} = q_j^n + \Delta t \left(f_{j-1,out}^n - f_{j,inc}^n\right) = q_j^n + \Delta t \left(f_{j-1,out}^n - \frac{1}{\Delta t}\left[\Delta t' \mu_j + \left(\Delta t - \Delta t'\right) f_{j-1,out}^n\right]\right).$$

Then by (17), we have:

$$q^{n+1} = q_j^n + \Delta t f_{j-1,out}^n - \left[\Delta t' \mu_j + \left(\Delta t - \Delta t'\right) f_{j-1,out}^n\right] = q_j^n + \Delta t'(f_{j-1,out}^n - \mu_j) = 0.$$

■

Remark 4 *An alternative method to avoid negativity of queues is the use of adaptive time meshes, where Δt is replaced by $\Delta t'$ computed in (17).*
Alternatively, one may modify the equation for q with a relaxation term when the queue buffer is decreasing to zero. In other words q is exponentially decaying to zero when the queue is emptying. This gives rise to a nonlinear stiff equation and restrictions on the time steps must be carefully addressed, see [19].

3.2 Different space and time grid meshes

We now consider the possibility of choosing different space and/or time grid meshes. This is necessary in the general case in which L_j have not rational ratios, but can also be useful for computational complexity reduction, as we will see in Section 6.

3.2.1 Different space meshes for different suppliers

For each supplier $j \in \mathcal{J}$, the numerical grid in $[0, L_j] \times [0, T]$ is defined choosing a fixed time grid mesh Δt, then different space grid meshes are necessary. Set $\Delta x_j = v_j \Delta t$, where $v_j := \frac{L_j}{T_j}$ indicates the processing velocity. Then, grid points are $(x_i, t^n)_j = (i\Delta x_j, n\Delta t)$, $i = 0, ..., N_j$, $n = 0, ..., \eta_j$. The Upwind scheme for the parts density of the arc j now reads:

$${}^j\rho_i^{n+1} = {}^j\rho_i^n - \frac{\Delta t}{\Delta x_j} v_j \left({}^j\rho_i^n - {}^j\rho_{i-1}^n\right), \; j \in \mathcal{J}, \; i = 0, ..., N_j, n = 0, ..., \eta_j. \tag{19}$$

The CFL condition (see [23]) is automatically satisfied since:

$$\Delta t = \min\left\{\frac{\Delta x_j}{v_j} : j \in \mathcal{J}\right\}. \tag{20}$$

For queues we refer again to equation (14).
In case of negative values of queues, fluxes corrections have to be considered, which are the same as in Section 3.1.

3.2.2 Different time meshes for different suppliers

We now consider the case of different temporal meshes (and same space meshes). Fix two consecutive arcs $j-1$ and j, then two different numerical grids are defined, whose points are, respectively:

$$(x_k, t^{n_{j-1}})_{j-1} = (k\Delta x, n_{j-1}\Delta t_{j-1}),\ k = 0, .., N_{j-1},\ n_{j-1} = 0, ..., \eta_{j-1},$$
$$\left({}^{j}x_k, t^{n_j}\right) = (k\Delta x, n_j\Delta t_j),\ k = 0, .., N_j,\ n_j = 0, ..., \eta_j.$$

For the queue buffer occupancy the explicit Euler is given by:

$$q_j^{n_j+1} = q_j^{n_j} + \Delta t_j\left(f_{j-1,out}^{n_j} - f_{j,inc}^{n_j}\right). \tag{21}$$

where $f_{j,inc}^{n_j}$ is computed as in (15), while $f_{j-1,out}^{n_j}$ must be suitably defined. If $\Delta t_{j-1} < \Delta t_j$, we define $m(n_j)$ and $M(n_j)$ as:

$$m(n_j) = \sup\{m : m\Delta t_{j-1} \le n_j\Delta t_j\};$$
$$M(n_j) = \inf\{M : M\Delta t_{j-1} \ge (n_j+1)\Delta t_j\},$$

and set

$$f_{j-1,out}^{n_j} = \sum_{l=1}^{M(n_j)-m(n_j)-1} \Delta t_{j-1} f_{j-1}({}^{j-1}\rho_{N_{j-1}}^{m(n_j)+l})$$
$$+ \left[(m(n_j)+1)\Delta t_{j-1} - n_j\Delta t_j\right] f_{j-1}({}^{j-1}\rho_{N_{j-1}}^{m(n_j)}) +$$
$$+ \left[(n_j+1)\Delta t_j - (M(n_j)-1)\Delta t_{j-1}\right] f_{j-1}({}^{j-1}\rho_{N_{j-1}}^{M(n_j)-1}).$$

Notice that, in the special case $\Delta t_j = \gamma\Delta t_{j-1}$, $\gamma \in \mathbb{N} \setminus \{1\}$, we simply have:

$$f_{j-1,out}^{n_j} = \sum_{l=1}^{M(n_j)-m(n_j)-1} \Delta t_{j-1} f_{j-1}({}^{j-1}\rho_{N_{j-1}}^{m(n_j)+l}) = \sum_{l=1}^{\gamma} \Delta t_{j-1} f_{j-1}({}^{j-1}\rho_{N_{j-1}}^{\gamma n_j+l}).$$

If, on the contrary, $\Delta t_{j-1} > \Delta t_j$, we set

$$f_{j-1,out}^{n_j} = f_{j-1}^{\left\lfloor \frac{n_j\Delta t_j}{\Delta t_{j-1}} \right\rfloor},$$

where $\lfloor\cdot\rfloor$ indicates the floor function.

CFL conditions now reads:

$$\Delta t_j \le \frac{\Delta x}{v_j}, \qquad j = 1, \ldots, N.$$

In case of negative values of queues, fluxes corrections have to be considered. The modifications w.r.t. Section 3.1 can be easily computed and are omitted for sake of space.

4 Convergence

The aim of this Section is to study the convergence of the Upwind-Euler numerical scheme. The main idea is to compare numerical solutions with those produced by a Wave Front Tracking algorithm and control the norm of generalized tangent vectors which measure the distance, as in [21].

We consider a Cauchy problem of the type (4)-(8), with initial conditions $\rho_{j,0}$ in BV, the space of bounded variation functions. Fix an initial space meshes Δx_0 and define a sequence of approximate solutions ${}^{\nu,j}\rho_i^n$, generated sampling the initial datum $\rho_{j,0}$ on grids with space meshes $\Delta x_{j,\nu} = 2^{-\nu}\Delta x_{j,0}$ and using the time meshes:

$$\Delta t_{j,\nu} = \frac{\Delta x_{j,\nu}}{v_j} = 2^{-\nu}\frac{\Delta x_{j,0}}{v_j}, \tag{22}$$

where v_j is the velocity of the j-th suppliers, thus granting the CFL conditions. More precisely:

$${}^{\nu,j}\rho_i^0 = \rho_{j,0}\big((a_j + i\,2^{-\nu}\Delta x_{j,0})\ +\big)$$

where $(\cdot\ +)$ indicates the limit from the right, which exists because of the assumption of BV initial data. We can define a projection of the approximate solution over the space of piecewise constant functions by setting:

$$\pi_{PC}\left({}^{\nu,j}\rho^n\right) = \sum_{i=0}^{L_j/2^{-\nu}\Delta x_{j,0}-1} {}^{\nu,j}\rho_i^n\,\chi_{[a_j+i\,2^{-\nu}\Delta x_{j,0},\,a_j+(i+1)2^{-\nu}\Delta x_{j,0}[}$$

where $\chi_{[a,b]}$ is the indicator function of the set $[a,b]$.
We define the corresponding queue buffer occupancy approximations ${}^{\nu}q_j^n$ as specified in the previous Section and consider the projection over piecewise linear function:

$$\pi_{PL}\left({}^{\nu}q_j\right)(t) = {}^{\nu}q_j^n + (t - n\Delta t_{j,\nu})({}^{\nu}q_j^{n+1} - {}^{\nu}q_j^n) \qquad \text{for } t \in [n\Delta t_{j,\nu}, (n+1)\Delta t_{j,\nu}[.$$

We will also consider the Wave Front Tracking (briefly WFT) solution ${}^{j}\rho_\nu^{WFT}$ starting from the initial datum

$$\pi_{PC}\left({}^{\nu,j}\rho^0\right).$$

Roughly speaking, a WFT solution is obtained in the following way:

- Solve the Riemann problems corresponding to discontinuities of $\pi_{PC}\left({}^{\nu,j}\rho_i^0\right)$;
- Use the piecewise constant solution obtained piecing together the solutions to Riemann problems up to the first time of interaction of two shocks;
- Then solve a new Riemann problem created by interaction of waves and prolong the solution up to next interaction time, and so on.

To ensure the existence of WFT solutions and their convergence, it is enough to control the number of waves, interactions and the BV norm. This is easily done in scalar case since both the number of waves and the BV norm are decreasing in time. We refer the

reader to [4] for details.
For queues we use the exact solutions to (6) and indicate them by ${}^{\nu}q_j^{WFT}$. BV estimates for complete ODE-PDE model (4)-(8) are proved in [21].

For a general WFT scheme we should replace, in solutions to Riemann problems, possible rarefactions by a set of small non entropic shocks of size $2^{-\nu}$. However, in our case rarefactions do not show up because the flux is piecewise linear. Let us describe in detail solutions to Riemann problems.
Fix a supplier j and consider a Riemann problem with initial data (ρ_-, ρ_+). Then we have to distinguish some cases:

- $\rho_- < \mu_j$. In this case the solution is given by a shock travelling with velocity $\lambda = \frac{f_j(\rho_+) - f_j(\rho_-)}{\rho_+ - \rho_-}$ (which equals v_j in case $\rho_+ \leq \mu_j$).
- $\rho_- = \mu_j$. Then the solution is a shock travelling with velocity v_j if $\rho_+ < \mu_j$ and with zero velocity if $\rho_+ > \mu_j$.
- $\rho_- > \mu_j$. If $\rho_+ \geq \mu_j$ then the solution is a shock with zero velocity. Otherwise, the solution is formed by a first shock (ρ_-, μ_j) travelling with zero velocity and a second shock (μ_j, ρ_+) travelling with velocity v_j.

Notice that as soon as a boundary datum will achieve a value below μ_j, then in finite time all values above μ_j will disappear from the j-th supplier, see also [21]. Therefore, for simplicity, we will assume

$$\rho_{j,0}(x) \leq \mu_j. \tag{23}$$

Then the same inequality will be satisfied for all times both for the numerical approximation and wave front tracking ones, i.e.:

$$\pi_{PC}\left({}^{\nu,j}\rho^n\right)(x) \leq \mu_j \qquad \text{for all } n \geq 0,\ x \in [a_j, b_j], \tag{24}$$

$${}^{j}\rho_{\nu}^{WFT}(t,x) \leq \mu_j \qquad \text{for all } t \geq 0,\ x \in [a_j, b_j]. \tag{25}$$

In this case solutions to Riemann problems are particularly simple, indeed the conservation law is linear, thus given some Riemann data (ρ_-, ρ_+) on the j-th supplier, the solution is always given by a shock travelling with velocity v_j. Therefore, the WFT solution will differ from the projected numerical ones only for effects due to queues dynamics.

To prove convergence of the numerical scheme, we thus compare the projected numerical solution $(\pi_{PC}\left({}^{\nu,j}\rho^n\right), \pi_{PL}({}^{\nu}q_j))$ with the wave front tracking solution $({}^{j}\rho_{\nu}^{WFT}, {}^{\nu}q_j^{WFT})$. More precisely we consider their difference as expressed by a generalized tangent vector, i.e. write:

$$\pi_{PC}\left({}^{\nu,j}\rho^n\right)(t) = {}^{j}\rho_{\nu}^{WFT}(t) + \sum_{\alpha \in A_j(t)} \xi_\alpha(t) \Delta\rho_\alpha(t), \tag{26}$$

$$\pi_{PL}({}^{\nu}q_j)(t) = {}^{\nu}q_j^{WFT}(t) + \eta_j(t), \tag{27}$$

where $A_j(t)$ is the set of discontinuities of ${}^{j}\rho_{\nu}^{WFT}$ at time t and $\Delta\rho_\alpha$ the strength of the given discontinuity (i.e. the value of the jump). In other words the part density $\pi_{PC}\left({}^{\nu,j}\rho^n\right)(t)$ is obtained from ${}^{j}\rho_{\nu}^{WFT}(t)$ shifting the shocks of quantities ξ_α, while $\pi_{PL}({}^{\nu}q_j)(t)$ is obtained from ${}^{\nu}q_j^{WFT}$ shifting its value of $\eta_j(t)$. We use the symbol $(\xi, \eta)_\nu$

to indicate the collection of all tangent vectors over all suppliers.
This approach was used in [21] to study uniqueness and continuous dependence of solutions. We report the general construction in the Appendix for reader's convenience. The norms of tangent vectors to WFT solutions are proved to be decreasing in time as stated in Lemma 8 of the Appendix (for a proof see [21]).
Our idea is to study the evolution of tangent vectors defined in (26)-(27) to estimate the increase in time of their norms defined as:

$$\|(\xi,\eta)_\nu(t)\| = \sum_j \sum_{\alpha\in A_j(t)} |\xi_\alpha \Delta\rho_\alpha| + \sum_j |\eta_j(t)|.$$

Notice that:

$$\|(\xi,\eta)_\nu(t)\| = \sum_j \|\pi_{PC}\left({}^{\nu,j}\rho^n\right)(t) - {}^j\rho_\nu^{WFT}(t)\|_{L^1} + \sum_j |\pi_{PL}({}^\nu q_j)(t) - {}^\nu q_j^{WFT}(t)|. \quad (28)$$

First of all the evolution inside suppliers of tangent vectors is the same as for the part densities, i.e. shifts evolves travelling at velocity v_j on the j-th supplier, and no increase of norms occur. Such increase may occur in three cases:

- Interaction of a wave with an empty queue;
- Interaction of a wave with a non empty queue;
- Emptying of a queue.

Let us start analyzing what happens when a wave interacts with an empty queue, say the j-th queue. Let us call ξ_-, $\Delta\rho_-$, η^-, respectively ξ_+, $\Delta\rho_+$, η^+, the values of jump shift, jump and queue shift before, respectively after, the interaction. The shifted wave interacts with the queue with a time delay given by $\delta t = \frac{\xi_-}{v_{j-1}}$ and the new shift is given by $\xi_+ = v_j\,\delta t = \frac{v_j}{v_{j-1}}\xi_-$. Since the queue is empty before the interaction, we have $\eta_- = 0$, while $\eta^+ = (\Delta\rho_- - \Delta\rho_+)\xi_-$. Therefore

$$|\xi_+\,\Delta\rho_+| + |\eta^+| = |\xi_-|\left(\frac{v_j}{v_{j-1}}|\Delta\rho_+| + |\Delta\rho_- - \Delta\rho_+|\right) \le \max\left\{\frac{v_j}{v_{j-1}}, 1\right\}|\xi_-\,\Delta\rho_-|, \quad (29)$$

where we used the fact that $\Delta\rho_-$ and $\Delta\rho_+$ have the same sign.
Let us now consider the interaction with a nonempty queue. Calling ξ_-, $\Delta\rho_-$ the values of shifts and jumps before the interaction and by η^+ the produced shift in the queue, we simply get:

$$\eta^+ = \xi_-\Delta\rho_-, \quad (30)$$

thus the norm of the tangent vector is constant.
We now focus on the case of the j-th queue emptying at some time $\bar t \in [n\Delta t_{j,\nu}, (n+1)\Delta t_{j,\nu}[$, i.e the queue buffer has positive values in a left neighborhood of $\bar t$ and vanishes in a right neighborhood of $\bar t$. Then the WFT solution will generate a wave on the j-th supplier starting at time $\bar t$, while the projected numerical solution will generate two waves at times

$n\Delta t_{j,\nu}$ and $(n+1)\Delta t_{j,\nu}$. More precisely at time $(n+1)\Delta t_{j,\nu}$, in a right neighborhood of the left endpoint a_j, we have:

$$ {}^{j}\rho_{\nu}^{WFT}((n+1)\Delta t_{j,\nu}, x) = \begin{cases} f_{j-1,out}^{n} & x \in [a_j, a_j + v_j(\bar{t} - n\Delta t_{j,\nu})[\\ \mu_j & x \in [a_j + v_j(\bar{t} - n\Delta t_{j,\nu}), a_j + 2\, v_j \Delta t_{j,\nu}] \end{cases}, $$

$$ \pi_{PC}\left({}^{\nu,j}\rho^{n+1}\right)(x) = \begin{cases} \rho^{*} & x \in [a_j, a_j + v_j \Delta t_{j,\nu}[\\ \mu_j & x \in [a_j + \Delta t_{j,\nu}, a_j + 2\, v_j \Delta t_{j,\nu}] \end{cases}, $$

where ρ^* is a value in the interval $[f_{j-1,out}^{n}, \mu_j]$ (notice that $f_{j-1,out}^{n} < \mu_j$ since we assumed that the queue is emptying). This situation can be detected by tangent vectors if we consider the discontinuity $(f_{j-1,out}^{n}, \mu_j)$ as splitted in two parts: $\alpha = (f_{j-1,out}^{n}, \rho^*)$ and $\beta = (\rho^*, \mu_j)$ considering the shifts $\xi_\alpha = -v_j(\bar{t} - n\Delta t_{j,\nu}) < 0$ and $\xi_\beta = v_j((n+1)\Delta t_{j,\nu} - \bar{t}) > 0$. These two shifts are caused because of the approximation and the relative norm of tangent vectors are estimated as follows:

$$ |\xi_\alpha \Delta\rho_\alpha| = v_j(\bar{t} - n\Delta t_{j,\nu})\,(\rho^* - f_{j-1,out}^{n}), $$

$$ |\xi_\beta \Delta\rho_\beta| = v_j((n+1)\Delta t_{j,\nu} - \bar{t})\,(\mu_j - \rho^*), $$

therefore we can write:

$$ |\xi_\alpha \Delta\rho_\alpha| + |\xi_\beta \Delta\rho_\beta| \leq \Delta t_{j,\nu}\,(\mu_j - f_{j-1,out}^{n}). \tag{31} $$

Finally we have:

Lemma 5 *Assume (23) holds true and consider the tangent vector $(\xi, \eta)_\nu$ defined by (26), (27). Then it holds:*

$$ \|(\xi, \eta)_\nu(t)\| \leq 2^{-\nu}\; K\; \left(\sum_j TV(\rho_{j,0}) + \sum_{j \geq 2} \max\{\mu_{j-1}, \mu_j\} \right), $$

where $TV(\cdot)$ indicates the total variation and

$$ K = \left(\max_j \frac{\Delta x_{j,0}}{v_j} \right) \left(\prod_{j=2}^{N} \max\left\{ \frac{v_j}{v_{j-1}}, 1 \right\} \right). \tag{32} $$

Proof. The norm of the tangent vector at initial time is zero. Then it may increase due to queues emptying. For the j-th queue, such increase, estimated by (31), is bounded by $\Delta t_{j,\nu}$ times the strengths of waves interacting with the queue, which in turn is bounded by the total variation of ${}^{j-1}\rho_{\nu}^{WFT}$. On the other side, from (23), we get (25) thus, from formula (2.10a) and (2.10b) at page 165 of [21], we have:

$$ \sum_j TV({}^{j}\rho_{\nu}^{WFT}(t)) \leq \sum_j TV(\rho_{j,0}) + \sum_{j \geq 2} \left| \frac{d^{\,\nu} q_j^{WFT}}{dt}(0) \right|. $$

Moreover, it holds:

$$\left|\frac{d\,{}^{\nu}q_j^{WFT}}{dt}(0)\right| \leq \max\{\mu_{j-1},\mu_j\}.$$

The norm of the tangent vector may further increase due to interactions of waves with queues, but such increase is estimated in (29) and (30). Therefore by (22) we conclude. ■
Since WFT approximations are converging to a solution to the ODE-PDE coupled model, as proved in [21], from Lemma 5 we get that also $(\pi_{PC}\left({}^{\nu,j}\rho^n\right), \pi_{PL}({}^{\nu}q_j))$ are converging to a solution.
We now want further to estimate the convergence rate. For this purpose, define the convergence error as:

$$\begin{aligned} E_\nu(n) &= \sum_j \sum_i 2^{-\nu}\Delta x_{j,0}\ \left|{}^{\nu,j}\rho_i^n - {}^{\nu+1,j}\rho_i^n\right| + \sum_j |{}^{\nu}q_j^n - {}^{\nu+1}q_j^n| \\ &= \sum_j \|\pi_{PC}\left({}^{\nu,j}\rho^n\right) - \pi_{PC}\left({}^{\nu+1,j}\rho^n\right)\|_{L^1} + \sum_j |{}^{\nu}q_j^n - {}^{\nu+1}q_j^n|. \end{aligned} \tag{33}$$

Moreover, we have:

$$E_\nu(0) = \sum_j \|{}^{j}\rho_\nu^{WFT}(0) - {}^{j}\rho_{\nu+1}^{WFT}(0)\|_{L^1} \leq 2^{-(\nu+1)}\sum_j \Delta x_{j,0}\, TV(\rho_{j,0}). \tag{34}$$

We then first estimate the increase of the distance between ${}^{j}\rho_\nu^{WFT}$ and ${}^{j}\rho_{\nu+1}^{WFT}$ in time. Notice that the initial datum ${}^{j}\rho_{\nu+1}^{WFT}(0) = \pi_{PC}\left({}^{\nu+1,j}\rho^0\right)$ can be obtained from ${}^{j}\rho_\nu^{WFT}(0) = \pi_{PC}\left({}^{\nu,j}\rho^0\right)$ by possibly shifting waves with tangent vectors with norms of the order $2^{-(\nu+1)}\Delta x_{j,0}$, in fact both functions are obtained sampling the same BV function on different subgrids. Then we can control the distance by Lemma 8 of the Appendix. More precisely:

$$\begin{aligned} \sum_j \|{}^{j}\rho_\nu^{WFT}(t) - {}^{j}\rho_{\nu+1}^{WFT}(t)\|_{L^1} \quad + \quad & \sum_j |{}^{\nu}q_j^{WFT}(t) - {}^{\nu+1}q_j^{WFT}(t)| \leq \\ & \sum_j \|{}^{j}\rho_\nu^{WFT}(0) - {}^{j}\rho_{\nu+1}^{WFT}(0)\|_{L^1}. \end{aligned} \tag{35}$$

Now the convergence error can be written as:

$$\begin{aligned} E_\nu(n) \leq\ & \|{}^{j}\rho_\nu^{WFT}(n\Delta t_\nu) - {}^{j}\rho_{\nu+1}^{WFT}(n\Delta t_\nu)\|_{L^1} + \sum_j |{}^{\nu}q_j^{WFT}(n\Delta t_\nu) - {}^{\nu+1}q_j^{WFT}(n\Delta t_\nu)| \\ +\ & \sum_j \|\pi_{PC}\left({}^{\nu,j}\rho^n\right)(t) - {}^{j}\rho_\nu^{WFT}(t)\|_{L^1} + \sum_j |\pi_{PL}({}^{\nu}q_j)(t) - {}^{\nu}q_j^{WFT}(t)| \\ +\ & \sum_j \|\pi_{PC}\left({}^{\nu+1,j}\rho^n\right)(t) - {}^{j}\rho_{\nu+1}^{WFT}(t)\|_{L^1} + \sum_j |\pi_{PL}({}^{\nu+1}q_j)(t) - {}^{\nu+1}q_j^{WFT}(t)|. \end{aligned}$$

Last four addenda can be estimated using (28) and Lemma 5. While the first two addenda are estimated using (35) and (34). Finally we get:

$$E_\nu(n) \leq 2^{-(\nu+1)}\sum_j \Delta x_{j,0}\, TV(\rho_{j,0}) + (2^{-\nu}+2^{-(\nu+1)})\, K\ \left(\sum_j TV(\rho_{j,0}) + \sum_{j\geq 2}\max\{\mu_{j-1},\mu_j\}\right)$$

$$= 2^{-\nu}\left(\frac{1}{2}\sum_j \Delta x_{j,0}\, TV(\rho_{j,0}) + \frac{3}{2}\; K\;\left(\sum_j TV(\rho_{j,0}) + \sum_{j\geq 2}\max\{\mu_{j-1},\mu_j\}\right)\right),$$

where K is defined in (32). Finally we get the following:

Theorem 6 *Assume that $\rho_{j,0}$ are BV functions, $\rho_{j,0}(x) \leq \mu_j$ for every x and (22) holds true. Then the convergence error $E_\nu(n)$ (defined in (33)) tends to zero uniformly in n with linear convergence rate in $\Delta x_{j,\nu} = 2^{-\nu}\Delta x_{j,0}$.*

5 Numerical tests : Part I

We present some simulation results to illustrate the outcome of methods and discussion of previous Sections. To fix notation, let us define:

- *ordinary method* (OM): Upwind scheme for densities, equation (12); Euler scheme for queues, equation (14);
- *different spatial steps method* (DSSM): Upwind scheme for densities, equation (19), with different CFL conditions, equation (20); Euler scheme for queues, equation (14);
- *different temporal steps method* (DTSM): Upwind method for densities, equation (12); modified Euler scheme for queues, equation (21).

5.1 First test - negative queue buffer occupancies

In this test we show the importance of flux corrections in case of oscillating queue buffer occupancies (see subsection 3.1).
Consider a supply chain with $N = 4$ suppliers and the following parameters: $L_j = T_j = 1$, $j = 1,..,4$; $\mu_1 = 99$, $\mu_2 = 12$, $\mu_3 = 10$, $\mu_4 = 8$. The initial conditions are: $\rho_{j,0} \equiv 0$, $j = 1,...,4$, $q_{j,0} = 0$, $j = 2,3,4$. A total simulation time $T = 300$ is considered and for the first arc the inflow profile is given by $f_1(t) = 7.5\left(1 + \sin\frac{3\pi t}{20}\right)$.
Figure 3 depicts the evolutions of uncorrected and corrected queue buffer occupancies $q_2(t)$, simulated by OM with $\Delta x = \Delta t = 0.2$. It shows that meaningful numerical errors occur if flux corrections are not used. At time $t = 270$, the relative difference among peaks of corrected and uncorrected queue buffer occupancies is about 29%. In terms of L^1 norm the relative error in about 44.4% for $t \in [270, 300]$.
An erroneous approximation of $q_2(t)$ has a cascade effect, affecting the evolution of parts density for the supplier 2, but then also $q_3(t)$, $q_4(t)$, $\rho_3(t,x)$ and $\rho_4(t,x)$. In Figure 4 $\rho_3(30,x)$ is depicted with and without correction. Notice that the presence of a negative $q_2(t)$ generated an evolution of $\rho_3(30,x)$ which is completely different from the real dynamic. At $x = 0.6$, the relative error in $\rho_3(30,x)$ is about 40%.

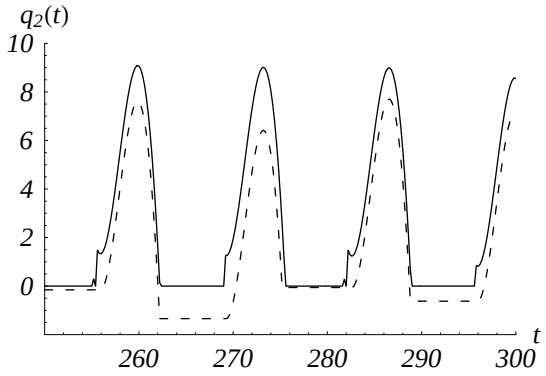

Figure 3: Queue buffer occupancy q_2: behaviour without flux correction (dashed line) and with flux correction (solid line).

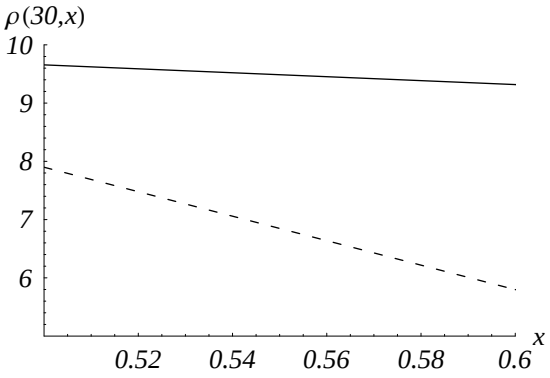

Figure 4: Behaviour of the density on the arc 3 at $t = 30$ with flux correction (dashed line) and without flux correction (continuous line).

5.2 Second test - different space and time meshes

We consider a supply chain with $N = 4$ suppliers. Maximal fluxes, processing times and lengths of each supplier are reported in the following table (see [17]):

supplier j	μ_j	T_j	L_j
1	25	1	1
2	15	1	0.2
3	10	3	0.6
4	15	1	0.2

We assume that all arcs are empty at $t = 0$, i.e. $\rho_{j,0} \equiv 0$; also queues at $t = 0$ are assumed empty: $q_{j,0} = 0$, $j = 2, 3, 4$. The total simulation time is $T = 140$. The inflow for the first supplier is given by:

$$f_1(t) = \begin{cases} \frac{18}{35}t, & 0 \le t \le \frac{T}{4}, \\ 36 - \frac{18}{35}t, & \frac{T}{4} < t < \frac{T}{2}, \\ 0, & \frac{T}{2} \le t \le T. \end{cases} \tag{36}$$

In Figure 5 (left), we present the simulation results for queue buffer occupancies, obtained by OM with $\Delta x = 0.0125$, $\Delta t = 0.5\Delta x$. Different behaviour for queues occur: q_4 remains empty as $\mu_4 > \mu_3$, while q_3 is higher than q_2 although processing velocities v_2 and v_3 are the same. We then run the same test for DSSM and DTSM, choosing, respectively,

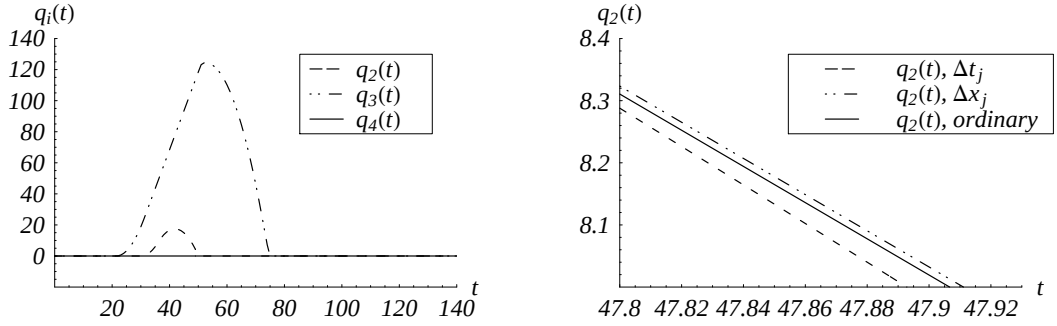

Figure 5: Behaviour of queues for OM (left) and comparison with other methods for q_2 (right).

$\Delta t = 0.0125$ and $\Delta x = 0.0125$. Other parameters for such methods are the same of OM. In Figure 5 (right), the behaviour of the queue buffer occupancy $q_2(t)$ is shown. Different numerical approximations give rise to very similar results.
A further analysis on CPU times (measured in seconds and computed by a Pentium 4, CPU 3.20 GHz, RAM 512 Mb) and convergence errors is made to compare methods. The following tables reports the obtained results.

Δx	**CPU**	L^1 errors
0.00625	1.703	0.001734
0.0125	0.156	0.079465
0.025	0.062	0.160575

TABLE 1: CPU times and L^1 errors for OM.

Δt	Δx_1	Δx_2	Δx_3	Δx_4	**CPU**	L^1 errors
0.00625	0.00625	0.00125	0.00125	0.00125	1.671	0.002911
0.0125	0.0125	0.0025	0.0025	0.0025	0.140	0.027847
0.025	0.025	0.005	0.005	0.005	0.046	0.132399

TABLE 2: CPU times and L^1 errors using DSSM.

Δx	Δt_1	Δt_2	Δt_3	Δt_4	**CPU**	L^1 errors
0.00625	0.0025	0.01875	0.0125	0.00625	0.828	0.003435
0.0125	0.05	0.00375	0.0025	0.00125	0.140	0.059411
0.025	0.1	0.075	0.05	0.025	0.046	0.127714

TABLE 3: CPU times and L^1 errors using DTSM.

We note that all previous tables contain no meaningful differences, for $\Delta x = 0.025$ and $\Delta x = 0.0125$, in terms of CPU times. Differences occur for the value $\Delta x = 0.00625$ for DTSM because of coarser grids used in three suppliers, thus at the price of less precision. As for L^1 errors, they are almost the same for OM, DSSM, and DTSM.
We conclude that, as expected, the considered methods have almost the same characteristics, as for goodness of approximation versus CPU times and L^1 errors.

6 Improvement of CPU times

In order to address the simulation of large networks, we aim at improving computational performances.

6.1 Logic pointer approach

Recall the Upwind scheme (12). If space and time grid sizes are set according to the relation $\Delta t_j = v_j \, \Delta x_j$ then ${}^j\rho_{i+1}^{n+1} = {}^j \rho_i^n$. In other words, the density values at time $n+1$ are obtained by those at time n by shifting of one position in the space grid. The computational complexity can be highly reduced by using a logic pointer, that allows to avoid the data shift in the vector of densities.
For a better comprehension of such strategy, consider a supplier of length L, divided into n segments. At $t = 0$, we suppose that the supplier is empty. At $t = 1$, the density value V_1 on the first segment is computed and the pointer is set to position 1. At $t = 2$, densities should be shifted while the new density value for the first segment, V_2, is computed. The physical shift inside the vector is not considered and the pointer is updated to the second position corresponding to V_2 (Figure 6), discarding the previous value and considering cyclic order in the vector. This operation is repeated until a time $t = n$, while at $t = n+1$ the new density is allocated in the first segment and the pointer is set back to position 1 and so on.

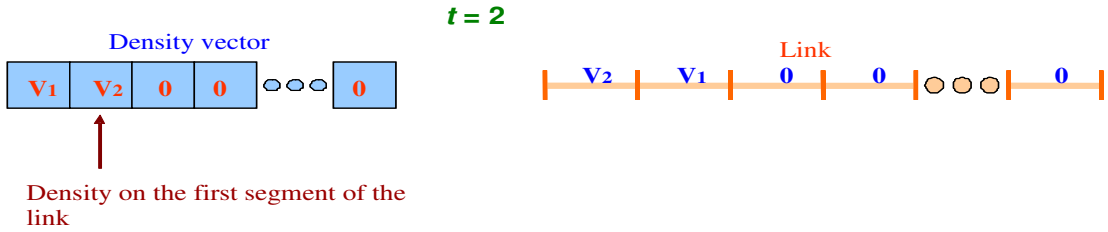

Figure 6: Situation at $t = 2$.

Operations and computational costs for OM and LP method are examined in the following table where # denotes the cardinality.

Operations	Computational costs
Densities	$\sim \sum_j \# \frac{L_j}{\Delta x_j}$
Boundary data	$\sim \#\mathcal{J} \times \frac{T}{\Delta t_j}$

Operations	Computational costs
Densities	$\sim \#\mathcal{J}$
Logic pointers	$\sim \#\mathcal{J}$
Boundary data	$\sim \#\mathcal{J} \times \frac{T}{\Delta t_j}$

TABLE 4: Computational costs for OM (left) and LP (right).

Notice that the update of densities for each supplier depends on space grid size for OM. Such dependence vanishes using the LP approach, while the cost of logic pointer update is fixed. Therefore, we get a substantial reduction of computational costs as illustrated in Section 7.

6.2 Different indices numeration

A concatenated list is used to store all informations about part densities on suppliers, each one identified by a sequential index. Then, informations for each link are obtained by a sequential research requiring a computational time directly proportional to the number N of suppliers. The computational complexity is $O(N)$ in the worst case, that occurs when the last arc of the list must be found.
In order to decrease the computational complexity, a vector, "Heap" whose $i-$th element identifies the $i-$ th arc by a pointer, is used. In this way, the generic arc i is found by a direct access to the $i-$ th position of the vector, $Heap[i]$. The numerical complexity of the research operation becomes $O(1)$, independently from the supply chain dimensions.

7 Numerical tests - Part II

We make an analysis of CPU times for the approaches described in Section 6.
Consider a sequential supply chain with four suppliers and the following parameters: $L_j =$

$T_j = 1$, $j = 1, 2, 3, 4$; $\mu_1 = 25$, $\mu_2 = 15$, $\mu_3 = 10$, $\mu_4 = 15$. We first use the method OM with different $\Delta x = \Delta t$, total simulation time $T = 140$, empty queues and arcs as initial condition and inflow profile for the first supplier as in (36). CPU times (measured in seconds and evaluated by a Pentium 4, CPU 3.20 GHz, RAM 512 Mb) and convergence orders are then compared with those of LP and DIN approaches. The following table shows the obtained results.

Numerical Code	$\Delta x = 0.00625$	$\Delta x = 0.0125$	$\Delta x = 0.025$
OM	**CPU** $= 0.359$, $\gamma = 0.982134$	**CPU** $= 0.109$, $\gamma = 0.991122$	**CPU** $= 0.046$, $\gamma = 0.946229$
LP	**CPU** $= 0.046$, $\gamma = 0.982134$	**CPU** $= 0.031$, $\gamma = 0.991122$	**CPU** $= 0.015$, $\gamma = 0.946229$
DIN + LP	**CPU** $= 0.031$ $\gamma = 0.982134$	**CPU** $= 0.015$, $\gamma = 0.991122$	**CPU** $= 0.015$, $\gamma = 0.946229$

TABLE 5: CPU times and convergence order (γ) for different numerical approaches.

We then considered a supply chain with $N = 10$ suppliers with the following parameters: $L_i = T_i = 1$, $i = 1, ..., 10$; $\mu_1 = 100$; $\mu_2 = 7$; $\mu_3 = 10$; $\mu_4 = 8$; $\mu_5 = 15$; $\mu_6 = 6$; $\mu_7 = 18$; $\mu_8 = 7$; $\mu_9 = 5$; $\mu_{10} = 9$. For OM we used different $\Delta x = \Delta t$, total simulation time $T = 140$, empty queues and arcs and input profile as in (36). CPU times (measured in seconds and evaluated by a Pentium 4, CPU 3.20 GHz, RAM 512 Mb) and convergence orders are again compared with those obtained by LP and DIN approaches. The following table summarizes the results.

Numerical Code	$\Delta x = 0.00625$	$\Delta x = 0.0125$	$\Delta x = 0.025$
OM	**CPU** $= 0.953$, $\gamma = 0.900810$	**CPU** $= 0.312$, $\gamma = 1.122965$	**CPU** $= 0.094$, $\gamma = 1.023330$
LP	**CPU** $= 0.140$, $\gamma = 0.900810$	**CPU** $= 0.078$, $\gamma = 1.122965$	**CPU** $= 0.046$, $\gamma = 1.023330$
DIN + LP	**CPU** $= 0.093$, $\gamma = 0.900810$	**CPU** $= 0.046$, $\gamma = 1.122965$	**CPU** $= 0.031$, $\gamma = 1.023330$

TABLE 6: CPU times and convergence order (γ) for different numerical approaches.

Convergence orders and the obtained numerical results for queues and densities are very similar for OM, LP, and DIN + LP. On the contrary, CPU time can decrease of up to 90% for the two last numerical approaches. This is more evident when the number of arcs of the supply chain is very large, as shown from the following simulation case. Consider a supply chain with $N = 100$ arcs, and the following characteristics: $L_i = T_i = 1$, $i = 1, ..., 100$; $\mu_1 = 100$; $\mu_i = 5$, $i = 2, ..., 100$. For OM we chose different $\Delta x = \Delta t$, total simulation time $T = 140$, empty arcs and queues and input profile as in (36). CPU times (measured in seconds and evaluated by a Pentium 4, CPU 2 GHz, RAM 2 GHz) are compared with those obtained by LP and DIN approaches. The following table reports

the obtained results.

Numerical Code	$\Delta x = 0.00625$	$\Delta x = 0.0125$	$\Delta x = 0.025$
OM	14.406	5.719	2.515
LP	5.500	2.906	1.500
DIN + LP	0.953	0.562	0.265

TABLE 7: CPU times for different numerical approaches.

Appendix

Let us first focus on the ρ_js: a "generalized tangent vector" consists of two components (v, ξ), where $v \in L^1$ describes the L^1 infinitesimal displacement, while $\xi \in \mathbb{R}^n$ describes the infinitesimal displacement of discontinuities. A family of piecewise constant functions $\theta \to \rho^\theta$, $\theta \in [0,1]$, with the same number of jumps say at the points $x_1^\theta < ... < x_M^\theta$, admits a tangent vector if the following functions are well defined:

$$L^1 \ni v^\theta(x) \doteq \lim_{h \to 0} \frac{\rho^{\theta+h}(x) - \rho^\theta(x)}{h},$$

and also the numbers

$$\xi_\beta^\theta \doteq \lim_{h \to 0} \frac{x_\beta^{\theta+h} - x_\beta^\theta}{h}, \qquad \beta = 1, ..., M.$$

Notice that the path $\theta \to \rho^\theta$ is not differentiable w.r.t. the usual differential structure of L^1, in fact if $\xi_\beta^\theta \neq 0$, as $h \to 0$ the ratio $\left[\rho^{\theta+h}(x) - \rho^\theta(x)\right]/h$ does not converge to any limit in L^1.
The L^1-length of the path $\gamma : \theta \to \rho^\theta$ is given by:

$$\|\gamma\|_{L^1} = \int_0^1 \left\|v^\theta\right\|_{L^1} d\theta + \sum_{\beta=1}^M \int_0^1 \left|\rho^\theta(x_\beta+) - \rho^\theta(x_\beta-)\right| \left|\xi_\beta^\theta\right| d\theta. \tag{37}$$

According to (37), the L^1-length of a path γ is also equal to the integral of the norm of its tangent vector, defined as follows:

$$\|(v,\xi)\| \doteq \|v\|_{L^1} + \sum_{\beta=1}^M |\Delta\rho_\beta| \, |\xi_\beta| \,,$$

where $\Delta\rho_\beta = \rho(x_\beta+) - \rho(x_\beta-)$ is the jump across the discontinuity x_β.

Now, given two piecewise constant functions ρ and ρ', call $\Omega(\rho, \rho')$ the family of all "differentiable" paths $\gamma : [0,1] \to \gamma(t)$ with $\gamma(0) = \rho$, $\gamma(1) = \rho'$. To define a Finsler type metric d, we set the distance between ρ and ρ' to be equal to

$$d(\rho, \rho') \doteq \inf \left\{ \|\gamma\|_{L^1}, \gamma \in \Omega(\rho, \rho') \right\}.$$

To define d on all L^1, for given $\rho, \rho' \in L^1$ we set

$$d(\rho, \rho') \doteq \inf \left\{ \|\gamma\|_{L^1} + \|\rho - \tilde{\rho}\|_{L^1} + \left\|\rho' - \tilde{\rho}'\right\|_{L^1} : \right.$$
$$\left. \tilde{\rho}, \tilde{\rho}' \text{ piecewise constant functions}, \gamma \in \Omega(\rho, \rho') \right\}.$$

It is easy to check that this metric coincides with the usual L^1 metric.

Remark 7 *Since the Finsler type metric d coincides with the usual L^1 metric, the reader could think that the whole framework is not so useful. On the contrary, the different differential structure permits to rely on tangent vectors, whose norm can be easily controlled. This would not be possible using the tangent vectors of the usual differential structure of L^1, i.e. having only the v component.*
Also, while for systems of conservation laws it is possible to find a decreasing functional, this is not the case for networks (see [15]), even for a scalar conservation law.

Let us now turn to the supply-chains case. It is easy to see that all paths in L^1 connecting piecewise constant functions can be realized using only the ξ component of the tangent vector, see [5]. Therefore, indicating by $x_{\beta_i^j}$ the positions of discontinuities, $j = 1, \dots, N$, $i = 1, \dots, M_j$, a tangent vector to a function defined on the network is given by:

$$(\xi_{\beta_i^j}, \eta_j),$$

where $\xi_{\beta_i^j}$ is the shift of the discontinuity $x_{\beta_i^j}$, while η_j is the shift of the queue buffer occupancy q_j. The norm of a tangent vector is given by:

$$\|(\xi_{\beta_i^j}, \eta_j)\| = \sum_{j,i} |\xi_{\beta_i^j}||\Delta\rho_{\beta_i^j}| + \sum_j |\eta_j|.$$

Again, to control the distance among solutions it is enough to control the evolution of norms of tangent vectors. Finally, we have:

Lemma 8 *The norm of tangent vectors are decreasing along wave front tracking approximations.*

References

[1] D. Armbruster, P. Degond, C. Ringhofer, A model for the dynamics of large queueing networks and supply chains, SIAM Journal on Applied Mathematics, 66 (3), pp. 896 - 920, 2006.

[2] D. Armbruster, P. Degond, C. Ringhofer, Kinetic and fluid models for supply chains supporting policy attributes, Transportation Theory Statist. Phys., 2006b.

[3] D. Armbruster, D. Marthaler, C. Ringhofer, Kinetic and fluid model hierarchies for supply chains, SIAM J. on Multiscale Modeling, 2 (1), pp. 43 - 61, 2004.

[4] A. Bressan, Hyperbolic Systems of Conservation Laws - The One - dimensional Cauchy Problem, Oxford Univ. Press, 2000.

[5] A. Bressan, G. Crasta, B. Piccoli, Well-Posedness of the Cauchy Problem for $n \times n$ Systems of Conservation Laws, Memoirs of the American Mathematical Society, vol. 146, n. 694 (2000).

[6] G.Bretti, R. Natalini, B. Piccoli, Numerical approximations of a traffic flow model on networks, Networks and Heterogeneous Media 1(1), pp. 57-84, 2006.

[7] G. Bretti, C. D'Apice, R. Manzo, B. Piccoli, A continuum - discrete model for supply chains dynamics, Networks and Heterogeneous Media (NHM), 2 (4), pp. 661 - 694, 2007.

[8] G. Bretti, B. Piccoli, A tracking algorithm for car paths on road networks, SIAM J. on Appl. Dyn. Syst. 7, pp. 510-531, 2008.

[9] C. Dafermos, Hyperbolic Conservation Laws in Continuum Physics, Springer - Verlag, 1999.

[10] C. Daganzo, A Theory of Supply Chains, Springer Verlag, New York, Berlin, Heidelberg, 2003.

[11] C. D'Apice, R. Manzo, A fluid dynamic model for supply chains, Networks and Heterogeneous Media (NHM), 1 (3), pp. 379 - 398, 2006.

[12] C. D'Apice, R. Manzo, B. Piccoli, Modelling supply networks with partial differential equations, to appear on Quarterly of Applied Mathematics.

[13] D. Helbing, S. Lämmer, T. Seidel, P. Seba, T. Platkowski, Physics, stability and dynamics of supply networks, Physical Review E 70 (2004), 066116.

[14] D. Helbing, S. Lämmer, Supply and production networks: from the bullwhip effect to business cycles, in: D. Armbruster, A. S. Mikhailov, and K. Kaneko (eds.) Networks of Interacting Machines: Production Organization in Complex Industrial Systems and Biological Cells, World Scientific, Singapore, 2005, pp. 33 - 66.

[15] M. Garavello and B. Piccoli, Traffic flow on networks, Applied Math Series Vol. 1, American Institute of Mathematical Sciences, 2006.

[16] S. K. Godunov, A finite difference method for the numerical computation of discontinous solutions of the equations of fluid dynamics, Mat. Sb. 47, 1959, pp. 271 - 290.

[17] S. Göttlich, M. Herty, A. Klar, Network models for supply chains, Communication in Mathematical Sciences, 3(4), pp. 545 - 559, 2005.

[18] S. Göttlich, M. Herty, A. Klar, Modelling and optimization of Supply Chains on Complex Networks, Communication in Mathematical Sciences, 4(2), pp. 315 - 330, 2006.

[19] S. Göttlich, M. Herty, C. Ringhofer, Optimization of order policies in supply networks, European J. Oper. Res. 202(2), pp. 456-465, 2010.

[20] M. Herty, A. Klar, Modeling, Simulation, and Optimization of Traffic Flow Networks, SIAM J. Sci. Comput. 25(3), pp. 1066-1087, 2003

[21] M. Herty, A. Klar, B. Piccoli, Existence of solutions for supply chain models based on partial differential equations, SIAM J. Math. An., 39(1), pp. 160 - 173, 2007.

[22] C. Kirchner, M. Herty, S. Göttlich and A. Klar, Optimal control for continuous supply network models, Netw. Heterog. Media 1(4), pp. 675 - 688 ,2006.

[23] R. J. Leveque, Finite Volume Methods for Hyperbolic Problems, Cambdrige, 2002.

[24] T. Nagatini, D. Helbing, Stability analysis and stabilization strategics for linear supply chains, Physica A: Statistical and Theoretical Physics, 335 (3-4), pp. 644 - 660, 2004.